

Geophysical Research Letters

RESEARCH LETTER

10.1029/2018GL078157

Special Section:

Cassini's Final Year: Science
Highlights and Discoveries

Key Points:

- Both poles have warm cyclonic vortices with 100-mbar temperatures increasing by 7 K within 1.2 degrees of the pole
- Temperatures are consistent with subsidence of 0.05 mm/s at 100 mbar extending down to at least 500 mbar
- Temperature gradients imply that the cyclonic winds decay with altitude over three scale heights in the upper troposphere and stratosphere

Correspondence to:

R. K. Achterberg,
Richard.K.Achterberg@nasa.gov

Citation:

Achterberg, R. K., Flasar, F. M., Bjoraker, G. L., Hesman, B. E., Gorius, N. J. P., Mamoutkine, A. A., et al. (2018). Thermal emission from Saturn's polar cyclones. *Geophysical Research Letters*, 45, 5312–5319. <https://doi.org/10.1029/2018GL078157>

Received 3 APR 2018




Accepted 7 MAY 2018

Accepted article online 17 MAY 2018

Published online 5 JUN 2018

©2018. American Geophysical Union.
All Rights Reserved.
This article has been contributed to by
US Government employees and their
work is in the public domain in the USA.

Thermal Emission From Saturn's Polar Cyclones

R. K. Achterberg^{1,2} , F. M. Flasar², G. L. Bjoraker², B. E. Hesman³, N. J. P. Gorius⁴,
A. A. Mamoutkine^{5,6}, L. N. Fletcher⁷ , M. E. Segura¹ , S. G. Edgington⁸, and S. M. Brooks⁸

¹Department of Astronomy, University of Maryland, College Park, MD, USA, ²Planetary Systems Laboratory, NASA Goddard Space Flight Center, Greenbelt, MD, USA, ³Space Telescope Science Institute, Baltimore, MD, USA, ⁴Department of Mechanical Engineering, The Catholic University of America, Washington, DC, USA, ⁵ADNET Systems Inc., Bethesda, MD, USA, ⁶Now at Department of Astronomy, University of Maryland, College Park, MD, USA, ⁷Department of Physics and Astronomy, University of Leicester, Leicester, UK, ⁸Jet Propulsion Laboratory, California Institute of Technology, Pasadena, CA, USA

Abstract We have used data from the Cassini Composite Infrared Spectrometer to map the temperatures in Saturn's polar cyclones at the highest spatial resolution obtained during the Cassini mission. We find temperature contrasts of 7 K in the upper troposphere within 1.4° of both poles, roughly 50 percent larger than earlier measurements at lower spatial resolution. The polar hot spots weaken with depth, disappearing near 500 mbar. In the stratosphere, the polar hot spot becomes broader, extending 4° from the poles, and weakens with altitude disappearing near 1 mbar. A thermal relaxation model shows that the tropospheric hot spot is consistent with adiabatic heating from subsidence with a vertical velocity of about −0.05 mm/s above 500 mbar. The observed temperature gradients imply that the winds in the polar cyclone decay with increasing altitude over roughly three pressure scale heights above the 200-mbar level.

Plain Language Summary We have used data from the Composite Infrared Spectrometer to map the temperatures in Saturn's polar cyclones during the Cassini mission. The final orbits of the mission enabled the highest spatial resolution data (20 km) of the mission. The analysis of this data reveals temperature contrasts of 7 °C (11°F) in the upper troposphere within 1.4° of both poles which is roughly 50% larger than measurements taken at lower spatial resolution earlier in the mission. We find that the polar hot spot temperature contrast weakens with depth in the troposphere. It was discovered that the hot spot temperature contrast in the stratosphere is broader than seen in the troposphere and weakens with increased altitude. The tropospheric temperature contrasts can be explained by slowly descending vertical winds at a rate of 0.05 mm/s. We observed that the temperature gradients are consistent with rapidly decaying winds over increasing altitude at the tropopause.

1. Introduction

Thermal infrared observations of Saturn taken from Keck observatory in February 2004 (early southern summer) revealed the presence of a compact hot spot at Saturn's south pole, with a temperature increase within 3° of the south pole of 2.5 K at 100 mbar and 1 K at 3 mbar (Orton & Yanamandra-Fisher, 2005). Subsequent observations from the Composite Infrared Spectrometer (CIRS) onboard the Cassini Orbiter (Fletcher et al., 2008, 2015) confirmed the existence of hot spots with temperature contrasts of up to 5 K within 2° to 3° of latitude of both poles in the upper troposphere and middle stratosphere, indicating that the polar hot spot is not a seasonal phenomenon.

Imaging at visible and near-infrared wavelengths by the Cassini Imaging Science Subsystem and Visible and Infrared Mapping Spectrometer shows that the polar hot spots are associated with strong cyclonic polar vortices, with peak zonal wind velocities in excess of 150 m/s near ±88.7° planetographic latitude and a local maximum in vorticity at the pole (Antuñano et al., 2015, 2018; Baines et al., 2009; Dyudina et al., 2008, 2009; Sánchez-Lavega et al., 2006; Sayanagi et al., 2017).

The structure of the polar vortices in visible imaging bears a striking similarity to a terrestrial hurricane, with a central eye of 1.5° to 2° radius surrounded by cyclonically spiraling clouds extending up to 6° from the poles. The south polar vortex has two distinct eyewalls, at 89.1° S and 88.3° S, with cloud altitudes changing abruptly

Table 1*Proximal Orbit Observations of Saturn's Polar Vortices From CIRS*

Observation	Start time	Duration (h:mm)	Latitude coverage	Spectral resolution (cm^{-1})	Spatial resolution (degree of arc)	No. of spectra	
						FP1	FP3/4
271SA_HIRESWACS001	2017-116T06:30:00	2:20	87°N–90°N	2.7	0.05–0.10	226	830
271SA_HIRESWACS002	2017-116T09:10:00	1:54	86°S–90°S	2.7	0.09–0.14	192	875
271SA_REGMAP001	2017-116T11:04:00	3:26	86°S–90°S	2.7	0.10–0.21	836	2,920
281SA_REGMAP001	2017-180T14:16:00	6:00	80°N–90°N	2.7	0.04–0.19	1,517	7,275
281SA_HIRESWACS002	2017-180T22:22:00	1:54	87.5°S–90°S	2.7	0.07–0.08	133	590
289SA_REGMAP001	2017-232T16:15:27	1:38	87.5°S–90°S	15.5	0.04–0.06	1,126	5,000

by 40 and 70 km, respectively (Dyudina et al., 2009). The north polar vortex has a more complicated, and temporally variable, cloud structure, with a relatively bright region of spiraling clouds between 89.3°N and 89.7°N surrounded by a dark ring extending to 89.1°N (Antuñano et al., 2018; Sanz-Requena et al., 2018; Sayanagi et al., 2017). Images in methane band filters, which are sensitive to the amount of upper tropospheric haze, show a dark spot at both poles extending to 88.7°, indicating a hole in the tropospheric haze (Sayanagi et al., 2017). The cloud and haze structure, as well as the warm core, of the vortex can be explained by subsidence within the vortex.

The geometry of the Cassini proximal orbits allowed for targeted observations of Saturn's poles within 1.5 to 6 hr of Cassini's closest approach to Saturn, at distances to the pole down to $\sim 1 R_S$, giving spatial resolutions with CIRS as low as 0.04° of arc (~ 20 km). The resolution of these observations is an order of magnitude better than the mapping observations used by Fletcher et al. (2008, 2015), giving CIRS an unprecedented view of Saturn's polar cyclones in the thermal infrared.

2. Data

Cassini CIRS is a Fourier transform spectrometer covering the spectral range from 10 to 1,500 cm^{-1} (6.7–1,000 μm) with a spectral resolution adjustable between 0.5 and 15.5 cm^{-1} . The spectral range is covered by three focal planes: Focal plane 1 (FP1), covering 10 to 600 cm^{-1} , is a single detector with an approximately Gaussian spatial response with a diameter projected on the sky of 3.9 mrad and a full width at half maximum of 2.5 mrad. Focal planes 3 and 4 (FP3 and FP4), covering 600 to 1,100 cm^{-1} and 1,050 to 1,500 cm^{-1} , respectively, are 1-by-10 linear arrays with each pixel having a square response of 0.27 mrad. The instrument and its operation are described in detail by Jennings et al. (2017) and Flasar et al. (2004).

During the proximal orbit phase of the Cassini mission, CIRS observations of the poles were obtained during three periapse periods: rev 271 (26 April 2017), rev 281 (29 June 2017), and rev 289 (20 August 2017; south pole only). During these observations the inbound leg came in near the north pole, and the outbound leg passed near the south pole. The CIRS focal planes were swept meridionally across the pole in a direction perpendicular to the FP3/4 arrays. FP3 and FP4 were operated in paired mode, with data from adjacent pairs of pixels electrically summed onboard the instrument for increased signal-to-noise ratio, except for the north polar observation on rev 281 which used single pixels for increased spatial resolution. The observations on revs 271 and 281 were taken at a Hamming-apodized spectral resolution of 2.7 cm^{-1} , while the observation on rev 289 was at a spectral resolution of 15.5 cm^{-1} . The spatial resolution during the observations varied between roughly 0.04° and 0.2° of arc in FP3 and FP4, a factor of 10 to 20 higher resolution than the routine temperature mapping observations during the Cassini mission used by Fletcher et al. (2008, 2015) and a factor of 5 better than the south polar observation used by Dyudina et al. (2009). FP1 data have a spatial resolution (FWHM of the approximately Gaussian field of view) of 5 worse than FP3/FP4. A summary of the observations is given in Table 1.

Because of Cassini's orbital geometry during the proximal orbits, during the period near periapse Saturn and its rings filled a substantial part of the field of view of the passive radiator used to cool the P3 and FP4 detector assembly to its normal operating temperature of 76 K. As a result, the FP3 and FP4 detectors were at an elevated temperature during the outbound south pole observations, resulting in lowered sensitivity and an

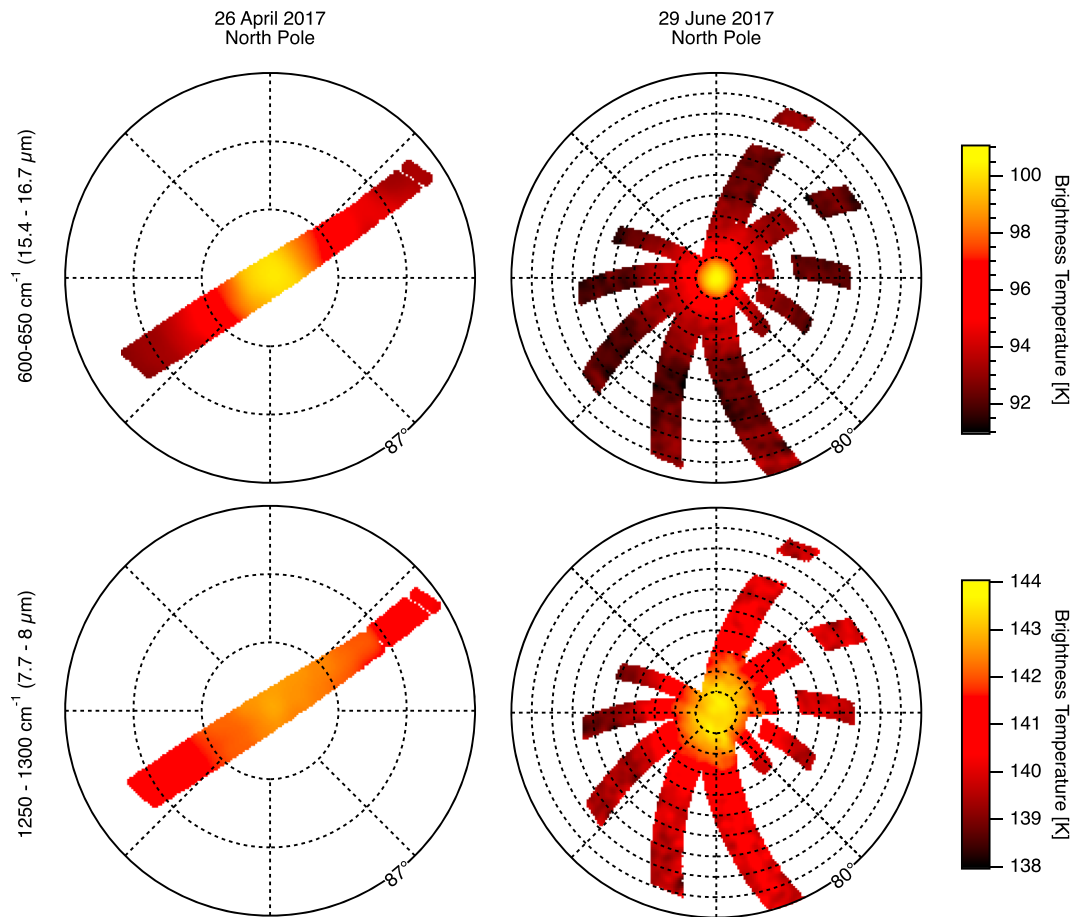


Figure 1. Polar orthographic projection maps of brightness temperatures at Saturn's north pole, averaged over 600–650 cm^{-1} (top row) and 1,250–1,300 cm^{-1} (bottom row), from observations on 26 April 2017 (left column) and 29 June 2017 (right column). Latitude circles are shown (dashed lines) at 1° intervals.

increased noise level. Combined with the lower atmospheric temperatures at the south (winter) pole, the south polar observations have considerably lower signal-to-noise level than the north polar observations.

3. Analysis and Results

Information on atmospheric temperatures comes from three parts of the observed spectra. In FP4, the ν_4 methane band between 1,200 and 1,400 cm^{-1} is sensitive to temperatures in the midstratosphere between about 0.5 and 5 mbar. In FP3, the continuum between 600 and $\sim 670 \text{ cm}^{-1}$, from collision-induced absorption (CIA) of $\text{H}_2\text{-H}_2$, $\text{H}_2\text{-He}$, and $\text{H}_2\text{-CH}_4$ pairs, is sensitive to the temperature in a narrow pressure region around 100 mbar in the upper troposphere. In FP1, the hydrogen CIA continuum between 220 and 600 cm^{-1} is sensitive to temperatures between roughly 100 and 400 mbar; temperatures at pressures up to about 600 mbar can be obtained from longer wavelengths (50 to 230 cm^{-1}) if the rotational absorption lines of ammonia and phosphine are modeled.

Figure 1 shows a polar orthographic projection map of brightness temperatures from the two north polar maps, calculated from radiances averaged over the range 600 to 650 cm^{-1} , which is indicative of temperatures in the upper troposphere near 100 mbar and averaged over 1,250 to 1,300 cm^{-1} , which is indicative of temperatures in the midstratosphere near 4 mbar. The tropospheric images show the compact hot spot at the northern pole, with a temperature increase of nearly 7 K within 1.5° (1,700 km) of the pole (seen more clearly in Figure 2 below), with the temperature gradient extending to the pole within the resolution of the observations. As in earlier observations (Fletcher et al., 2008, 2015) the hot spot is broader and weaker in the midstratosphere than in the upper troposphere.

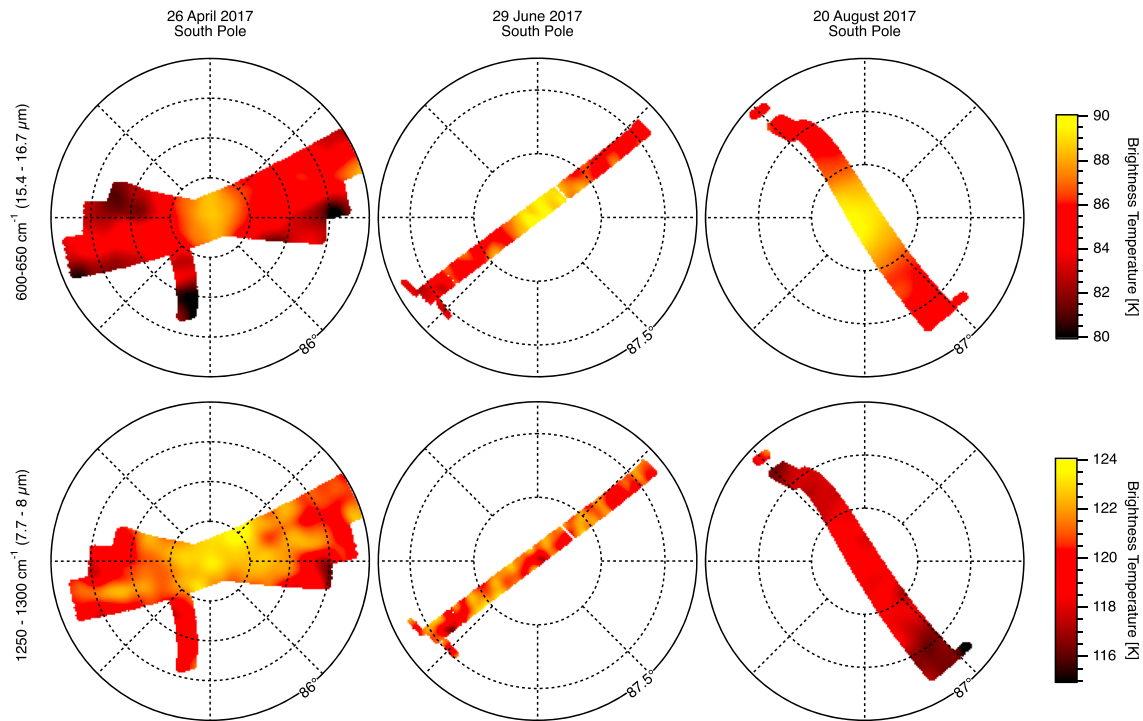


Figure 2. Polar orthographic projection maps of brightness temperatures at Saturn's south pole, averaged over $600\text{--}650\text{ cm}^{-1}$ (top row) and $1,250\text{--}1,300\text{ cm}^{-1}$ (bottom row), from observations on 26 April 2017 (left column) and 29 June 2017 (middle column), and 20 August 2017 (right column). Latitude circles are shown (dashed lines) at 1° intervals.

Similar maps of the three south polar observations are shown in Figure 3. Although the data are considerably noisier than for the north pole, the south polar troposphere shows a hot spot of similar size, but slightly lower amplitude, as the north. A stratospheric hot spot is not visible in the maps; however, the noise level of the data is very high and we will see below from temperature retrievals of zonally averaged data that a weak stratospheric hot spot is present at the south pole.

To retrieve temperatures, we use the north polar map from 29 June 2017 and the south polar map from 26 April 2017, which have the greatest latitude coverage for each pole, as well as scans at multiple longitudes. For each map, the spectra from FP3 and FP4 were zonally averaged in 0.2° wide latitude bins centered every 0.1° in latitude, while the FP1 spectra were zonally averaged in 0.5° bins centered every 0.25° of latitude. Temperatures were retrieved from the averaged spectra using the constrained linear inversion algorithm described by Conrath et al. (1998), with separate retrievals for data from each focal plane. The forward model uses 199 layers equally spaced in log pressure between 5 bar and $1\ \mu\text{bar}$. The opacity sources used are the CIA opacity from $\text{H}_2\text{--H}_2$, $\text{H}_2\text{--He}$, and $\text{H}_2\text{--CH}_4$ pairs, methane absorption from the ν_4 band in FP4, and the rotational lines of NH_3 and PH_3 in FP1. The CIA opacity is calculated according to Borysow et al. (1985), Borysow and Frommhold (1986), and Borysow et al. (1988). Molecular band absorption is calculated using the correlated- k approximation (Goody et al., 1989; Lacis & Oinas, 1991) with opacity tables precalculated using the opacity data described by Fletcher et al. (2012, Table 4). The initial guess atmosphere is the same as Achterberg et al. (2014), with the addition of CH_4 using the profile of Moses et al. (2000) scaled to a tropospheric mole fraction of 4.7×10^{-3} (Fletcher et al., 2009).

FP4 retrievals are performed first, using the spectral range from $1,250$ to $1,310\text{ cm}^{-1}$, and give temperature profiles valid between roughly 0.5 and 5 mbar, blending in to the initial guess profile at higher and lower pressures. The temperature profiles from the FP4 retrievals are then used as the initial guess temperatures for the FP3 and FP1 retrievals. The FP3 retrievals use the spectral range from 600 to 660 cm^{-1} and give temperatures in a layer roughly one scale height thick centered near 100 mbar. The FP1 retrievals use the spectral range from 50 to 550 cm^{-1} , and temperature, hydrogen para-fraction, NH_3 mole fraction, and PH_3 mole fraction are retrieved as described by Achterberg et al. (2014). The resulting temperature profiles are valid between roughly 100 and 600 mbar.

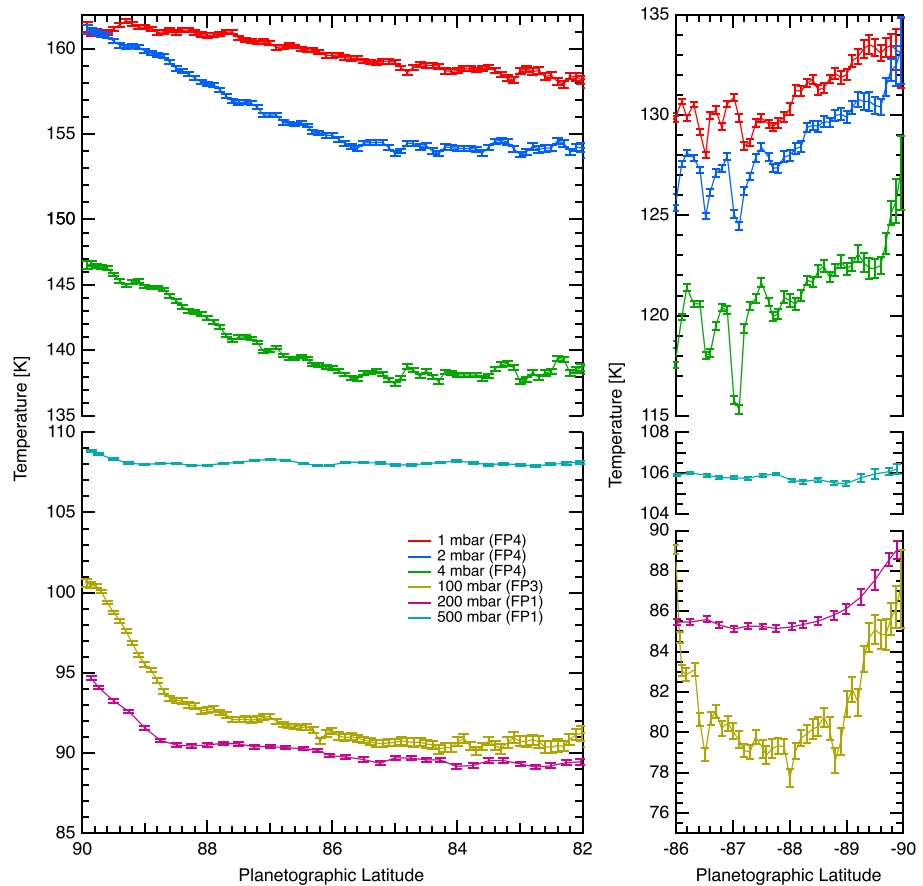


Figure 3. Zonal mean temperatures retrieved from the north polar map on 29 June 2017 (left) and the south polar map on 26 April 2017 (right). Error bars indicate uncertainty from propagation of random noise in the spectra.

The resulting temperatures at several pressure levels are shown in Figure 3. At the north pole, the temperatures near 100 mbar show a 10-K increase between 84°N and the pole, with 7 K of that increase within 1.4° (1,600 km) of the pole. There is a noticeable inflection point in the meridional temperature gradient near 88.6°N, poleward of which the temperature gradient persists to within 0.2° of the pole. The hot spot weakens with increasing pressure, disappearing near 500 mbar. In the midstratosphere, the polar hot spot is broader, with the inflection in dT/dy occurring at 86°N for pressures greater than about 1 mbar. The amplitude of the polar heating decreases rapidly between 2 and 1 mbar, and at 1 mbar we see only the northernmost part of the broader stratospheric polar warming seen in the summer hemisphere (Fletcher et al., 2015). The south polar tropospheric hot spot is similar to that in the north, with an 8-K temperature increase between 88°S and the pole, though without the sharp inflection point in the meridional gradient. In the south polar stratosphere, 4-mbar temperatures show a compact hot spot at the pole, with $\Delta T \sim 4$ K within 0.5° (600 km) of the pole, which is weaker at 2 mbar and gone at 1 mbar, as well as an ~ 4 -K temperature increase between 86°S and 89.5°S. The latitudinal coverage of the south polar observations used here is insufficient to show the full extent of the broader stratospheric cyclone, but Fletcher et al. (2015) found a local minimum in the 5-mbar temperatures at about 85°S from CIRS data through 2014.

4. Discussion

4.1. Vertical Winds

The warm temperatures, as well as the lower cloud altitudes and opacities, and clearing of the tropospheric haze within the polar vortices, can be explained by atmospheric subsidence and adiabatic heating (Dyudina et al., 2009; Fletcher et al., 2008, 2015). The amount of subsidence required to produce the observed temperature gradients can be estimated by considering the potential temperature, the temperature a parcel of gas would have if compressed or expanded to a reference pressure at constant entropy, which is an advectively

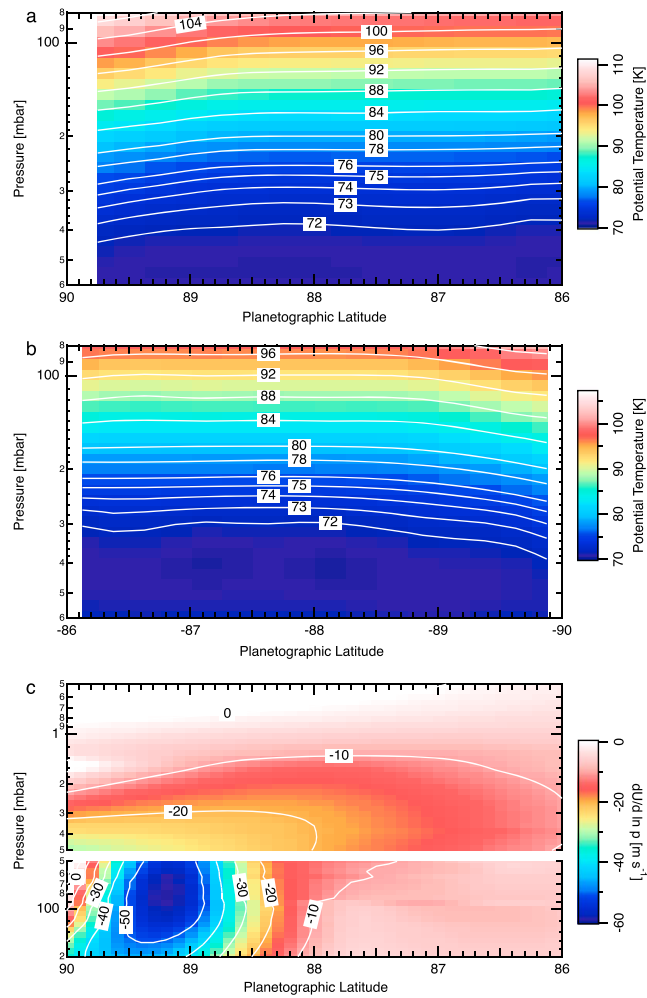


Figure 4. (a) Potential temperature retrieved from FP1 for the north polar observation on 29 June 2017. (b) Potential temperature retrieved from FP1 for the south polar observation on 26 April 2017. Potential temperatures use a reference pressure of 100 mbar. (c) Vertical gradient of the mean zonal wind calculated from the FP3/4 retrieved temperatures using the thermal wind approximation, for the north polar observation on 29 June 2017. There is a gap between 5 and 50 mbar, because the data are not sensitive to temperatures in this region.

conserved quantity in the absence of nonadiabatic heating or cooling. Figure 4 shows cross sections of potential temperature, calculated from temperatures retrieved from FP1 for the rev 281 north polar observation and the rev 271 south polar observation calculated as described by Gierasch et al. (2004). The potential temperature contours are depressed over both poles, indicating subsidence. They remain nearly parallel over the 100- to 600-mbar pressure range of the retrievals, implying that the vertical displacement is uniform through the upper troposphere. The minimum displacement needed to produce the observed temperature contrast can be estimated by assuming adiabatic descent and dividing the meridional temperature contrast ΔT by the difference between the observed and adiabatic vertical temperature gradients, $\partial T/\partial z + g/C_p$. Here z is altitude, g is the gravitational acceleration, and C_p is the specific heat. At around 100 mbar, we observe that $\Delta T \approx 7$ K, and from the retrieved FP1 temperature profiles, we calculate $dT/dz + g/C_p \approx 1.2$ K/km, giving a vertical displacement of ~ 6 km, or 0.2 of the pressure scale height at 100 mbar, consistent with the potential temperature contours in Figure 4.

Of course, the vertical displacement can be larger, but then the adiabatic heating must be balanced by diabatic heating or cooling. The simplest approximation is the zonally averaged energy equation with radiative relaxation expressed in terms of a Newtonian cooling time scale τ_R (e.g., Andrews et al., 1987):

$$w \left(\frac{\partial T}{\partial z} + \frac{g}{C_p} \right) = - \frac{T - T_{eq}}{\tau_R}, \quad (1)$$

where w is the vertical velocity, g is the gravitational acceleration, C_p is the specific heat, and T_{eq} is the radiative equilibrium temperature. Equation (1) assumes that the temporal variation and meridional advection of heat are small, so that vertical advection of heat is balanced by radiative heating or cooling, represented by relaxation to an equilibrium temperature, and applies to the zonal mean velocity and temperature. Localized vertical velocities can be much larger, in particular in areas of active convection. To estimate τ_R , we use the methodology of Fels (1982) for scale-dependent cooling rates. Assuming cooling from CIA of H_2 - H_2 , H_2 - He , and H_2 - CH_4 pairs and from the rovibrational bands of C_2H_2 , C_2H_6 , and CH_4 , we find values of τ_R^{-1} of about $6 \times 10^{-9} \text{ s}^{-1}$ in the upper troposphere for sinusoidal disturbances with a vertical wavelength of several scale heights. Assuming the observed temperature difference of 10 K between 85°N and the pole is indicative of $T - T_{\text{eq}}$ and $dT/dz + g/c_p = 1.2 \text{ K}$ as above; a zonal mean vertical velocity on the order of $w \sim -0.05 \text{ mm/s}$ near 200 mbar is needed to produce the observed polar hot spot. This gives an advective time scale for the meridional circulation associated with the vortex of $H/w \approx 20$ years. This time scale is comparable to the Saturn year, and long compared to the radiative time scale, as well as the predicted time scale for equilibration of the ortho and para states of hydrogen (Conrath & Gierasch, 1984); thus, a more accurate estimation of the meridional circulation associated with the polar vortex will need to include both seasonal radiative effects and the latent heat associated with equilibration of the hydrogen rotational state.

4.2. Thermal Wind Shear

Assuming geostrophic balance, where the meridional pressure gradient is balanced by the Coriolis force, the meridional temperature gradient is related to the vertical gradient of the zonal wind through the thermal wind relation:

$$\frac{\partial u}{\partial \ln p} = \frac{R}{f} \frac{\partial T}{\partial y}, \quad (2)$$

where p is the pressure, R is the gas constant, and $f = 2\Omega \sin(\psi)$ is the Coriolis parameter with Ω the angular rotation rate of Saturn and ψ the latitude. Figure 4c shows the vertical gradient of the zonal mean wind, calculated from the temperatures retrieved from FP3/4 data for the north polar map on 29 June 2017. The meridional temperature gradient was evaluated from a smoothing spline fit through the observed $T(\psi)$ at each pressure (Dierckx, 1993) to prevent the result from being dominated by noise, so the resulting $du/d \ln p$ should be considered only a rough estimate.

In the upper troposphere, the vertical wind shear is around 50 to 60 m/s per scale height, indicating that the observed winds decay with altitude into the stratosphere over about three pressure scale heights, if the observed temperature gradient does not weaken too much in the lower stratosphere where CIRS data have little sensitivity to temperature. In the middle stratosphere, the vertical wind shear extends over a larger latitude range than in the troposphere, and weakens rapidly with altitude, disappearing at about 1 mbar.

The 5- μm data from the Visual and Infrared Mapping Spectrometer (Baines et al., 2009) show that the north polar vortex extends downward to at least the 2-bar level with minimal decrease in amplitude, consistent with CIRS results that the temperature gradient disappears at 500 mbar, where the vertical temperature gradient becomes nearly adiabatic. The available data thus show that the winds associated with north polar vortex are roughly constant with altitude throughout much of the upper troposphere then decay with altitude through the uppermost tropopause and lower stratosphere.

5. Conclusions

CIRS observations of Saturn's polar cyclones at the highest spatial resolution obtained during the Cassini mission show temperature increase of roughly 7 K between $\pm 88.6^\circ$ and the poles in the upper troposphere near 100 mbar, with the temperature gradient persisting to within 0.1° of the pole. There is an abrupt inflection in the meridional temperature gradient at 88.6°N , roughly the location of the peak winds in the north polar cyclone. The observed temperature gradient weakens with depth, disappearing near the radiative-convective boundary near 500 mbar. In the middle stratosphere, the polar hot spots are broader than in the troposphere, extending to $\pm 86^\circ$, and weaken with increasing altitude, disappearing near 1 mbar.

The tropospheric temperature contrasts can be explained by subsidence within the polar vortices, with heating from adiabatic compression only partly balanced by radiative cooling. The required vertical velocity is roughly -0.05 mm/s , corresponding to an advective time scale of about 20 Earth years. Contours of potential

temperature are depressed at both poles by an amount that is independent of pressure, indicating that the subsidence extends down to at least 500 mbar with little change in amplitude. Application of thermal wind balance shows that the observed winds in the north polar cyclone decay with altitude at about 60 km/s per scale height, indicating that the cyclone weakens considerably in the lower stratosphere.

Acknowledgments

This work was supported by the NASA Cassini project. L. N. F. was supported by the Royal Society Research Fellowship and European Research Council Consolidator grant (under the European Union Horizon 2020 research and innovation programme, grant agreement 723890) at the University of Leicester. Calibrated spectra from Cassini CIRS are available from the Atmospheres Node of the Planetary Data System.

References

- Achterberg, R. K., Gierasch, P. J., Conrath, B. J., Fletcher, L. N., Hesman, B. E., Bjoraker, G. L., & Flasar, F. M. (2014). Changes to Saturn's zonal-mean tropospheric thermal structure after the 2010-2011 northern hemisphere storm. *The Astrophysical Journal*, *786*, 92. <https://doi.org/10.1088/0004-637X/786/2/92>
- Andrews, D. G., Holton, J. R., & Leovy, C. B. (1987). *Middle atmosphere dynamics*, *International Geophysical Series* (Vol. 40). Orlando: Academic Press.
- Antuñano, A., del Río-Gaztelurrutia, T., Sánchez-Lavega, A., & Hueso, R. (2015). Dynamics of Saturn's polar regions. *Journal of Geophysical Research: Planets*, *120*, 155–176. <https://doi.org/10.1002/2014JE004709>
- Antuñano, A., del Río-Gaztelurrutia, T., Sánchez-Lavega, A., & Rodríguez-Aseguinolaza, J. (2018). Cloud morphology and dynamics in Saturn's northern polar region. *Icarus*, *299*, 117–132. <https://doi.org/10.1016/j.icarus.2017.07.017>
- Baines, K. H., Momary, T. W., Fletcher, L. N., Showman, A. P., Roos-Serote, M., Brown, R. H., et al. (2009). Saturn's north polar cyclone and hexagon at depth revealed by Cassini/VIMS. *Planetary and Space Science*, *57*(14), 1671–1681. <https://doi.org/10.1016/j.pss.2009.06.026>
- Borysow, A., & Frommhold, L. (1986). Theoretical collision-induced rototranslational absorption spectra for the outer planets: H₂-CH₄ pairs. *The Astrophysical Journal*, *304*, 849–865. <https://doi.org/10.1086/164221>
- Borysow, J., Frommhold, L., & Birnbaum, G. (1988). Collision-induced rototranslational absorption spectra of H₂-He pairs at temperatures from 40 to 3000 K. *The Astrophysical Journal*, *326*, 509–515. <https://doi.org/10.1086/166112>
- Borysow, J., Trafton, L., Frommhold, L., & Birnbaum, G. (1985). Modeling of pressure-induced far-infrared absorption spectra: Molecular hydrogen pairs. *The Astrophysical Journal*, *296*, 644–654. <https://doi.org/10.1086/163482>
- Conrath, B. J., & Gierasch, P. J. (1984). Global variation of the para hydrogen fraction in Jupiter's atmosphere and implications for dynamics on the outer planets. *Icarus*, *57*, 184–204. [https://doi.org/10.1016/0019-1035\(84\)90065-4](https://doi.org/10.1016/0019-1035(84)90065-4)
- Conrath, B. J., Gierasch, P. J., & Ustinov, E. A. (1998). Thermal structure and para hydrogen fraction on the outer planets from Voyager IRIS measurements. *Icarus*, *135*, 501–517. <https://doi.org/10.1006/icar.1998.6000>
- Dierckx, P. (1993). *Curve and surface fitting with splines*. Oxford University Press. Monographs on Numerical Analysis.
- Dyudina, U. A., Ingersoll, A. P., Ewald, S. P., Vasavada, A. R., West, R. A., Baines, K. H., et al. (2009). Saturn's south polar vortex compared to other large vortices in the solar system. *Icarus*, *202*, 240–248. <https://doi.org/10.1016/j.icarus.2009.02.014>
- Dyudina, U. A., Ingersoll, A. P., Ewald, S. P., Vasavada, A. R., West, R. A., Del Genio, A. D., et al. (2008). Dynamics of Saturn's south polar vortex. *Science*, *319*, 1801. <https://doi.org/10.1126/science.1153633>
- Fels, S. B. (1982). A parameterization of scale-dependent radiative damping rates in the middle atmosphere. *Journal of the Atmospheric Sciences*, *39*, 1141–1152.
- Flasar, F. M., Kunde, V. G., Abbas, M. M., Achterberg, R. K., Ade, P., Barucci, A., et al. (2004). Exploring the Saturn system in the thermal infrared: The composite infrared spectrometer. *Space Science Reviews*, *115*, 169–297. <https://doi.org/10.1007/s11214-004-1454-9>
- Fletcher, L. N., Hesman, B. E., Achterberg, R. K., Irwin, P. G. J., Bjoraker, G., Gorius, N., et al. (2012). The origin and evolution of Saturn's 2011–2012 stratospheric vortex. *Icarus*, *221*, 560–586. <https://doi.org/10.1016/j.icarus.2012.08.024>
- Fletcher, L. N., Irwin, P. G. J., Orton, G. S., Teanby, N. A., Achterberg, R. K., Bjoraker, G. L., et al. (2008). Temperature and composition of Saturn's polar hot spots and hexagon. *Science*, *319*, 79–81. <https://doi.org/10.1126/science.1149514>
- Fletcher, L. N., Irwin, P. G. J., Sinclair, J. A., Orton, G. S., Giles, R. S., Hurley, J., et al. (2015). Seasonal evolution of Saturn's polar temperatures and composition. *Icarus*, *250*, 131–153. <https://doi.org/10.1016/j.icarus.2014.11.022>
- Fletcher, L. N., Orton, G. S., Teanby, N. A., Irwin, P. G. J., & Bjoraker, G. L. (2009). Methane and its isotopologues on Saturn from Cassini/CIRS observations. *Icarus*, *199*, 351–367. <https://doi.org/10.1016/j.icarus.2008.09.019>
- Gierasch, P. J., Conrath, B. J., & Read, P. L. (2004). Nonconservation of Ertel potential vorticity in hydrogen atmospheres. *Journal of the Atmospheric Sciences*, *61*, 1953–1965.
- Goody, R., West, R., Chen, L., & Crisp, D. (1989). The correlated-k method for radiation calculations in nonhomogeneous atmospheres. *Journal of Quantitative Spectroscopy and Radiative Transfer*, *42*(6), 539–550. [https://doi.org/10.1016/0022-4073\(89\)90044-7](https://doi.org/10.1016/0022-4073(89)90044-7)
- Jennings, D. E., Flasar, F. M., Kunde, V. G., Nixon, C. A., Segura, M. E., Romani, P. N., et al. (2017). The Composite Infrared Spectrometer (CIRS) on Cassini. *Applied Optics*, *56*(18), 5274–5294. <https://doi.org/10.1364/AO.56.005274>
- Lacis, A. A., & Oinas, V. (1991). A description of the correlated k distribution method for modeling nongray gaseous absorption, thermal emission, and multiple scattering in vertically inhomogeneous atmospheres. *Journal of Geophysical Research*, *96*(D5), 9027–9063.
- Moses, J., Bézard, B., Lellouch, E., Gladstone, G., Feuchtgruber, H., & Allen, M. (2000). Photochemistry of Saturn's atmosphere: I. Hydrocarbon chemistry and comparisons with iso observations. *Icarus*, *143*(2), 244–298.
- Orton, G. S., & Yanamandra-Fisher, P. A. (2005). Saturn's temperature field from high-resolution middle-infrared imaging. *Science*, *307*, 696–698. <https://doi.org/10.1126/science.1105730>
- Sánchez-Lavega, A., Hueso, R., Pérez-Hoyos, S., & Rojas, J. (2006). A strong vortex in Saturn's south pole. *Icarus*, *184*(2), 524–531. <https://doi.org/10.1016/j.icarus.2006.05.020>
- Sanz-Requena, J., Pérez-Hoyos, S., Sánchez-Lavega, A., Antuñano, A., & Irwin, P. G. (2018). Haze and cloud structure of Saturn's north pole and hexagon wave from Cassini/ISS imaging. *Icarus*, *305*, 284–300. <https://doi.org/10.1016/j.icarus.2017.12.043>
- Sayanagi, K. M., Blalock, J. J., Dyudina, U. A., Ewald, S. P., & Ingersoll, A. P. (2017). Cassini ISS observation of Saturn's north polar vortex and comparison to the south polar vortex. *Icarus*, *285*, 68–82. <https://doi.org/10.1016/j.icarus.2016.12.011>